Flight Envelope Determination Using Physically Motivated Margin Indicators for Unmanned Helicopters

Andreas E. Voigt
Research Scientist
German Aerospace Center
Braunschweig, Germany

Martin Laubner
Research Scientist
German Aerospace Center
Braunschweig, Germany

Johann C. Dauer
Research Scientist
German Aerospace Center
Braunschweig, Germany

ABSTRACT

Determining the flight envelope is a crucial step in the development process for Unmanned Aerial Vehicle (UAV). Research in the recent years focused on extending the useable flight envelope safely. As the number of available unmanned helicopters increases, maintaining low development costs is a key aspect to enable many civil business cases. Therefore, this paper presents a method to detect flight envelope limits tailored to commercially available unmanned helicopters. The proposed method consists of the following two steps: First, a set of dominating limiting effects of the flight envelope is identified and the concrete thresholds are determined. For the helicopter example used in this paper, these effects are engine power, actuator authority, rotor hub moments, load factor limitations, and the vortex ring state. Second, we propose to use indicators to measure the margin to these limits for each flight condition. A comprehensive rotorcraft model is used to calculate the indicators for the flight conditions. This model determines steady state responses or trim points. Thus, the margin for each trim point to the limit of the flight envelope can be estimated. In this paper, we apply this method to a helicopter in intermeshing rotor configuration and present a verification of the method. Furthermore, we compare the flight envelope of the proposed method to the known of this specific rotorcraft to assess the potential in respect of flight envelope expansion.

NOMENCLATURE

SYMBOLS

A	Area
d	Diameter of the rotor shaft
D	Deflection
E	Young modulus
F	Force
I	Second moment of inertia
Ind	Indicator
l	Free length
M	Moment
n	Load factor
P	Power
R	Material yield strength
S_f	Safety factor
S_m	Section modulus
T	Thrust
v_{iH}	Induced velocity in hover
u,v,w	Speeds in body-fixed frame
V_{zN}, V_{zX}, V_{xM}	Parameters used in vortex ring state model

GREEK SYMOLS

α_0	Bach coefficient
π	Pi
σ	Stress
τ_{xy}	Torsional stress

INDICES

B	Bending
BL	Lower boundary
BU	Upper boundary
C	Control deflection
E	Electric
H	Rotor hub loads
L	Left rotor
M	Rotor mast
Max	Maximum
n	Load factor
P	Power
R	Right rotor
T	Torsion
TS	Tail strike
VRS	Vortex ring state

INTRODUCTION

Determining the flight envelope is a key aspect for at least two field of work during the development of Unmanned Aerial Vehicle (UAV): First, the safe expansion of the flight envelope (FE), and second, during development of flight envelope protection means for care-free handling. In both fields, a reliable definition of the FE boundary is required to prevent any violation. For the case of flight envelope expansion, the UAV is equipped with a dedicated instrumentation to observe critical loads and parameters during flight. However, due to the particular low-cost requirements in the development process of many UAV's,

Presented at the Vertical Flight Society's 75th Annual Forum & Technology Display, Philadelphia, PA, USA, May 13-16, 2019.

the critical parameters are often not known and performing flight envelope expansion flights is thus difficult and error prone. An analogous problem is encountered during the development of the flight envelope protection systems. In this context, the definition of the boundary of the flight envelope is a compromise between flight safety and available flight performance. The more accurately the limiting effects of the FE are known, the larger is the usable flight envelope as Jeram pointed out in Ref. 1. Such limiting effects could be caused by structural, power or controllability limitations. Especially for new and uncommon aircraft configurations, this can be a challenging task. Therefore, a method to tackle these challenges is proposed in this paper.

The proposed approach is called flight envelope margin indicator (FEMI) method and it starts with comprehensively analyzing the potential limiting effects of the flight performance. An important characteristic of the presented approach is definition of the boundaries with physically motivated models similarly to those used during the design/preliminary design phase of the UAV. The flight envelope is derived from limits of mechanical loads, power or actuator authority or rates, c.f. Ref. 2 and 3; these values are also referred to as limit parameters. The limit parameters are calculated with first principle UAV models. In this paper, different FEMIs are introduced based on the limit parameters to describe the clearance or margin to the FE boundary. The subsequent FE is presented for an unmanned helicopter with two intermeshing rotors operated by DLR (the German Aerospace Center).

The remainder of the paper is structured as follows: first, an overview of limit detection methods available in literature is provided. Then, the basic principles of the proposed method are introduced; followed by the application of the limit margin indicators to the unmanned helicopter of DLR. In the last chapter, a simulation study with different model uncertainties is presented and the potential of the proposed method is shown by comparing the resulting FE to the one used so far.

RELATED WORK

The early envelope protection algorithms were incorporated in the flight control systems (FCS) to prohibit the pilot from exceeding the flight envelope. This is especially important in manned aviation with fly-by-wire systems due to a lack of tactile cue and the increasingly complex flight envelope boundaries as Yavrucuk pointed out in Ref. 2. For unmanned aircraft, flight envelope protection is an essential capability as well. A major field of work is the flight envelope limit detection or short limit detection. A variety of methods have been developed and applied to manned and unmanned systems, those are described in the following paragraphs.

Static flight envelope limits

Static flight envelope limits are often used for limit avoidance and are statically defined in the FCS design process, as mentioned in Refs. 2, 4, 5 . Different limiters define flight envelope boundaries, in simple cases, such as the maximum level flight speed or the maximum and minimum actuator deflection. The used limits are often defined as conservative constant values for maximum or minimum of the expected flight envelope. For example, the maximum horizontal speed is not adapted to the pressure altitude. Static flight envelope limits are well covered in literature, often easy to implement and therefore cost-efficient. However, such limits reduce the available flight performance due to the conservative representation of the flight envelope limits, see Ref. 6 .

Empiric limit models

Three possibilities to determine the limit parameters from empirical data are used. Firstly, there is offline identification of limit parameter models, which requires sufficient flight test data to identify a model that is valid for the whole flight envelope and determine corresponding parameters, see Refs. 7, 8**.** Secondly, the online detection of limit parameters is based on direct measurement of the current load, introduced in Ref. 9. Thirdly, an adaptive approach can be used using a model identified offline and improving the model capabilities by online measurements during flight. One example is the adaptive dynamic trim method introduced in Refs. 2 and 10. All three possibilities determine a functional relationship between the flight regime and commando input to the limit parameters. However, such identified models require a significant amount of flight test data for offline identification or a permanent instrumentation for online identification.

Physically motivated Models

Physically motivated models are based on a physical and often analytical description of the helicopter configuration. Such models are often called comprehensive rotor codes models and are used to determine the flight loads. Such models are used during the design phase of helicopters and the accuracy is generally sufficient for flight load analysis, see Ref. 11. The limit parameters can be determined from the calculated loads of the physically motivated model. However, such physical models are known to be less accurate than models identified from flight test data.

Hybrid models

A hybrid model is based on a physically motivated model but including empiric parameters to improve the accuracy, one example is given in Ref. 12. For such models, a good extrapolation capability can be assumed. However, generally at the boundaries of the flight envelope, nonlinear effects increasingly dominate the aircraft behavior the extrapolation capability degrades. Nevertheless, such models are used

during the design phase of the rotorcraft to determine flight mechanic characteristics and the preliminary flight envelope, see Ref. 12.

For flight envelope expansion, the basic assumption is that critical FE limiting effects are known, see Refs. 13 & 14, and are considered to be an output of the aircraft design process. In the case of the development of unmanned aircraft, maximum design loads are not always available or the mapping of the critical limit to the corresponding flight condition is missing as an output of the design process. For the case of limited system knowledge a flight envelope detection process was defined. In the following chapter other relevant challenges for such a flight envelope detection process are discussed.

CHALLENGES OF FLIGHT ENVELOPE DETECTION METHODS FOR UAV

An envelope detection method needs to take several UAV related issues into account:

Scalability of the method

Unmanned aircraft are very diverse and differ greatly in size, purpose and numbers of produced units. A short life span of aircraft versions can also be observed. Often, system components having an impact on the flight envelope change between these aircraft versions. From a manufacturer perspective, it is hence important to be able to tailor the effort to the lifespan and the development budget.

Definition of flight envelope boundaries

The flight envelope is generally considered to be the range of flight conditions in which the aircraft is operated. Such limitations are defined or determined during the design, development, and test phase of the aircraft. In manned aviation it is common to define flight envelopes with a safety margin to the real and possible critical limits of the aircraft in order to gain reaction time for the pilot. However, by doing so, the flight envelope and the subsequent flight performance is reduced. With the introduction of an inherent autopilot, the reaction time decreases significantly, compared to piloted aviation, providing the opportunity to drop some of the introduced safety margins.

Another aspect is the complexity of the flight envelope boundary itself. Often, the flight envelope limits are defined as a set of representative and derived parameters, like airspeed, altitude or climb rate, to be observable by the pilot. However, the flight envelope can be described more accurately by the limiting effect itself. Such flight envelope limiting effects can be structured in three groups: limits to structural load, the available engine power and control effectiveness, see Ref. 3. If the FE is defined according to the limiting effect, the subsequent flight performance is increased. Such limiting effects are for example: maximum hub loads, available engine power or control deflection authority.

Different flight dynamic requirements

There are significant differences in the requirements for envelope protection systems between civil and military UAV. Especially, agility is a crucial factor in military applications, e.g. if a fast and low level flight or a quick reaction to encounter a new threat is required. If a drone is used in a civil context, often agility is a minor factor to mission success.

In summary, automating the flight opens the opportunity to use envelope boundary descriptions clinging more naturally to the fundamental limiting effect.

PROPOSED FEMI BASED METHOD

To determine the flight envelope boundaries, a physically motivated first principle flight mechanic model is used. This model calculates the limit parameter values for different stationary flight conditions. The resulting limit parameter values are used to calculate limit margin indicators. These indicators are scaled to provide a value between 0% (if there is no load) and 100% (if the boundary is reached). Another significant characteristic is a steady gradient of the FEMI towards the boundary should be predominant to determine an approaching boundary.

1. Identification of limit parameters

To use this approach, first, the limit parameters need to be identified. For known configurations, the identification can be done using a list of reference limitations from literature or based on configuration similarities of other aircraft, see Refs. 6, 14, 13. If the used aircraft configuration is new and no or minor operational experience is available, a systematic approach helps to find all additional critical limit parameters. Such a systematic approach could be a breakdown of the aircraft into all flight critical elements and finding limiting effects for each. If a critical parameter is found and there is a realistic possibility to reach its maximum value during operation, it is defined as a limit parameter.

2. Determination of maximum acceptable parameter values

In a second step, the maximum value of each critical limit parameter is determined. Design and/or component test data is necessary for this task. If available, the design and test requirements as well as the derived component requirements including test loads and environmental conditions can be used to define maximum values.

3. Establishing a model from a comprehensive rotor code

In a third step, a model is formulated to calculate the limit parameter values under trim conditions. The used model has to represent the behavior of the rotorcraft at least for stationary and if possible also for transient flight conditions. The model uncertainties and limitations of the flight model should be known to subsequently calculate the limit margin indicators for the potential FE. For further calculation the model uncertainties are needed for all flight loads either as a functional relationship to the flight condition or as a maximum value.

4. Definition of the FEMI models

The development of the flight envelope limit margin indicator is the next step. For each limit parameter (or flight envelope limiting effect), a single margin indicator is developed. For the calculation of the FEMI models information from the design process as well as system specific empirical models can be used. The output of step 2 is used to normalize the indicator to 100% if the maximum acceptable value is reached. Per definition the indicator should not fall below 0%. The indicator should be a physically motivated function of the limit parameter it is based on. If possible, the indicator should have a continuous functional relation between inputs and outputs to enable gradient based flight envelope estimation.

5. Definition of the FE

In the last step, the flight envelope is found by evaluating the FEMI with the flight load calculated with the established model from step 3. A set of flight conditions is defined by sampling the optimistic range of the expected flight envelope. For this set of flight conditions, the flight loads are calculated. The maximum sustainable FEMI value is defined as the 100% reduced by the model uncertainties (see step 3). If all FEMIs of a flight condition are below the maximum sustainable FEMI value the flight condition is defined to be within the flight envelope. In case at least one FEMI is found to be greater than maximum sustainable FEMI value, the flight condition is declared outside of the flight envelope. Therefore within the flight envelope the indicator values vary between 0 % and the maximum sustainable FEMI value.

With this approach, a physically interpretable output is created and therefore, a deeper analysis can be performed in a terms of consequences of a possible limit violation. It is possible to completely define the flight envelope, if all limits are found and modeled.

Figure 1: DLR's unmanned helicopter superARTIS.

METHOD APPLIED TO DLR HELICOPTER

The superARTIS is a DLR-operated unmanned helicopter with a maximum take-off weight of 85 kg, see Figure 1. The helicopter has an intermeshing rotor configuration. It is equipped with a flight test instrumentation for structural and flight performance analysis, see Ref. 6, 15 for details.

Following the method introduced in the previous chapter, the first step is to find all potential flight envelope limiting effects. Therefore, a list of limiting parameters was created from literature see Ref. 14 and completed by previous operation experience with the superARTIS. The identified limit parameters are shown in Table 1. The identified limit parameters have been evaluated with simulations to determine if the limit could be violated. If so, the limit parameter was chosen to be implemented for the superARTIS. For example the actuator power was found to be a potential limitation, but after comparing the specifications and the simulated flight loads a safety factor of 7 was estimated. Consequently the actuator power was not chosen because it seemed not realistic to violate the actuator power limit.

Table 1: Limit parameter overview

Category	Limit parameter	Chosen
Structural load	Hub load	x
	Transmission torque	
	Blade bending load	
	Rotor clearance	x
	Vibratory load	
	Load factor	x
Controllability	Flight mechanic controllability	
	Actuator deflection rate	
	Actuator deflection authority	x
Available power	Engine power	x
	Actuator power	
Others	Vortex ring state	x

In this list of potential critical FE limitations, different classes of limits can be found. As an example, the limitation defined by the hub load is considered to be a direct limit due to its inevitable consequent effect if the boundary is violated. In contrast to the direct, the indirect limit does not have an inevitable effect, but will degrade capabilities of the aircraft, e.g the vortex ring state. This flight condition often challenges more than one limit parameter category. If operated in the vortex ring state, an increase in vibration together with a degraded controllability and increased power consumption can be observed. These identified limit parameters are generally independent with a few exceptions, like rotor clearance, hub moment, and vortex ring state.

In the second step, the maximum acceptable values for the limiting effects are determined. Therefore, design information in terms of sustainable loads for structure and components like the actuators is collected. The definition of the maximum values is difficult for the indirect limits. In case of the vortex ring state, a general model developed by Johnson can be found in the literature describing the boundaries of this flight condition, see Ref. 16. A different example is the fuel system of the superARTIS, which is designed for positive load factors only. Therefore, an indicator for a minimum load factor boundary of zero is set as a direct limit for the flight envelope.

In the third step, the flight mechanic model was created with the Helicopter Overall Simulation Tool (HOST). For a detailed description of HOST please see Ref. 11. The HOST Model of superARTIS comprises a variety of components, see Figure 2.

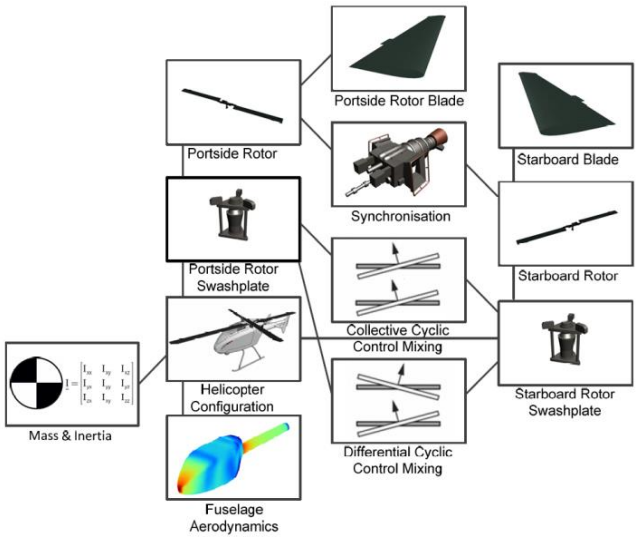

Figure 2: HOST model of superARTIS with components; from Ref. 6

HOST is able to calculate trim solutions from different equilibrium conditions, for example with constant translational and rotational acceleration. As an input for such calculations, the flight condition defined with the speed vector of the helicopter, the load factor, the gross weight, and other values like atmospheric parameters or initial trim values must be given. The output of the model and an overview is given in Figure 3.

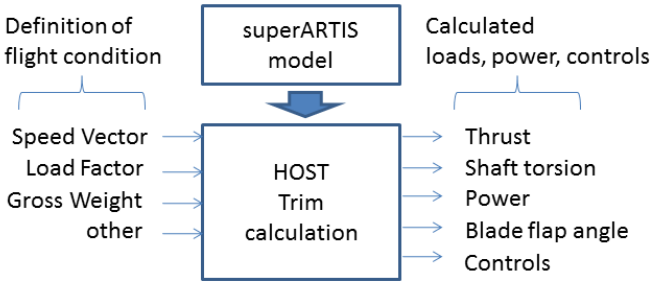

Figure 3: Illustration of the flight load calculation process

From the given list of limit parameters, six were implemented and the corresponding FEMIs were formulated. The other FE limiting effects are not considered, because either the maximum loads were never reached according to the HOST simulation or the limits are already sufficiently considered in the autopilot of the superARTIS. Therefore, the chosen and implemented indicators can be found in Table 1.

Limit margin indicators have been defined and developed for the implemented FE limiting effects. Further details can be found in the following chapter.

FEMI USED FOR DLR HELICOPTER

The defined FEMIs in this chapter are examples for the superARTIS. The calculations leading to the FEMI may be change with more flight test or system knowledge. The calculations should be regarded as examples to show the general formulation of the FEMIs.

Hub moment indicator

The hub load indicator is based on a simple tensile stress calculation taken from Ref. 17. It considers the mast bending, the rotor thrust as tension force and the torsion of the mast. The FEMI for the hub moment indicator is based on the Von Mises stress calculation 18 and 17. The calculation is based on a comparison of the maximum sustainable stress (σ_{max}) and the calculated or measured combined stress (σ)

$$\sigma = \sqrt{{\sigma_z}^2 + {\sigma_{xy}}^2 - \sigma_z\sigma_{xy} + 3(\alpha_0\tau_{xy})^2} \leq \sigma_{max}. \quad (1)$$

Here, σ_z denotes the stress of the rotor shaft in x-direction. It is approximately the rotor thrust direction assuming sufficiently small inclination of the rotor tip path plane. The stress induced by the mast bending is covered with σ_{xy} and the torsional load is represented by τ_{xy}.

Additionally, the empiric value α_0 is introduced to represent the dynamic behavior of the torsion loads. This coefficient α_0 is the material effort ratio; it describes the loading characteristic of the bending and torsional loads, see Ref 19. In this case, $\alpha_0 = 0.8$ is chosen to represent the oscillation of the peak-to-peak bending load in comparison to the relatively low peak-to-peak oscillation of the torsion. The shaft of the superARTIS is a solid material shaft. Therefore the cross section is a full circle. The tension force applied from the rotor can be represented with the following general term taken from Ref. 17

$$\sigma = \frac{F}{A}. \quad (2)$$

With *F* denoting the force later replaced by *T* to indicate the rotor thrust and *A* denoting the cross section area. Applied to the tension stress in z-axis(rotor shaft direction) the term is

$$\sigma_z = \frac{4T}{\pi d^2}, \quad (3)$$

with the rotor shaft diameter d. The stress resulting from the mast bending moment is referred to as σ_{xy}. And is also based on the same general term presented in formula 2, see Ref. 17. In this version the moment is denoted as M_B and the section modulus as S_m

$$\sigma = \frac{M_B}{S_m}. \quad (4)$$

The formula 4 applied to a solid material shaft results in a formulation of the shaft bending moment stress σ_{xy} by using

$$\sigma_{xy} = 32\frac{M_B}{\pi d^3}. \quad (5)$$

The third part of the hub loads is the stress as a result of the torsion load τ_{xy} can be written in a generally form as

$$\tau_{xy} = \frac{M_T}{S_m}, \quad (6)$$

with I_T denoting the second moment of area. Hence the τ_{xy} can be written as

$$\tau_{xy} = 32\frac{M_T}{\pi d^3}. \quad (7)$$

Additional forces representing the rotor drag or side forces can be implemented in a similar way. In this paper, however, they are assumed to be neglectable. The determined stress is normalized by the maximum sustainable stress and defines the first indicator (Ind_H)

$$Ind_H := \frac{\sigma}{\sigma_{max}}, \quad (8)$$

with

$$\sigma_{max} = \frac{R}{S_f}. \quad (9)$$

Here, *R* is the yield strength of the material and S_f is a safety factor with the value of 1.5 for steel, taken from Ref. 17.

Power indicator

Another limit margin indicator is the power indicator (Ind_P). It represents the maximum sustainable power output limit and is the sum of both rotors and the electric power produced by the generator. It is normalized by the maximum sustainable power of the engine (P_{Max}). Please note that the mechanical losses are not included. The rotors work with a fixed revolution per minute, therefore, the mechanical losses are considered to be approximately constant. Additionally, the maximum power P_{Max} is corrected for these losses. The indicator Ind_P can be considered slightly conservative, because P_{Max} is hence representing the worst case in terms of mechanical losses. The power indicator is calculated by

$$Ind_P := \frac{(P_L + P_R + P_E)}{P_{Max}}. \quad (10)$$

Here, the index L denotes the left rotor, the index R the right rotor, and P_E the consumed electric power.

Control deflection indicators

The control deflection indicators are calculated for every control axis, namely: pitch, roll, yaw and collective control. They are determined by normalizing the control deflection

D_C (commanded by the autopilot or from actuator feedback if available) with the maximum deflection D_{CMax}. The control defection indicators are defined by

$$Ind_C := \frac{D_C}{D_{CMax}}. \quad (11)$$

Rotor clearance indicator

The analysis to find limit parameters did show a potential of a tail strike as a result of aggressive command inputs. Therefore, the rotor clearance indicator (Ind_{RC}) was introduced. In an intermeshing configuration there are two possible ways to achieve yaw authority. First, with a differential pitch command of both rotors in opposite directions. Second, by a differential collective command for both rotors. The superARTIS used the first control scheme.

Thus mainly yaw and pitch command causes the blade to flap down and bend the rotor mast resulting in low a blade to vertical stabilizer clearance. Therefore, an indicator is formulated using the out of plane flap angle (β) at the azimuth (ψ) direction of the tail boom and the deflection of the rotor mast as a result of the bending moment (D_{MB})

$$Ind_{RC} := \frac{\beta(\psi) + D_{MB}(\psi)}{D_{TSMax}}. \quad (12)$$

While $\beta(\psi)$ is a direct output of the used HOST-model, the mast bending is a tensile stress calculation

$$D_{MB}(\psi) = \frac{M_B(\psi)\, l}{2\, E\, I}. \quad (13)$$

The second moment of inertia of the shaft against the bending load is denoted by I and E is the Young modulus of the used material of the shaft. The free shaft length l is used to determine the mast bending angle in radians.

Load factor indicator

The load factor indicator (Ind_n) was developed to protect the fuel system from negative load factors. A sigmoid function based on a hyperbolic tangent and the load factor n is used to determine the indicator. This function shows a close to linear behavior at the boundary (Ind_n=100%) and creates positive outputs during higher load factors than 0.

$$Ind_n := \tanh(-n) + 1. \quad (14)$$

In Figure 4 the function is depicted to show the linear behavior at the indicator of 100%.

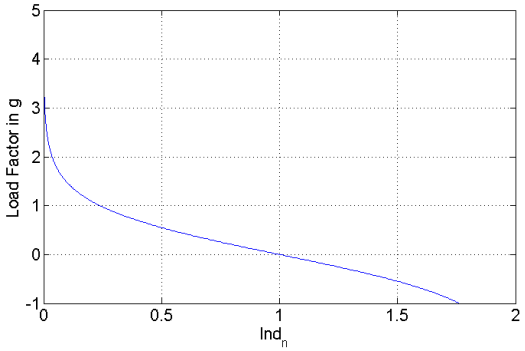

Figure 4: Load factor vs. Load factor indicator

Vortex ring state indicator

The vortex ring state is an indirect limitation of the FE. The calculation of the indicator is based on a model describing the boundaries of the vortex ring state developed by Johnson in Ref. 16**.** The model defines an upper and lower stability boundary for the vortex ring state for a single rotor. Here, we assume that the intermeshing configuration behaves similar to a single-main rotor configuration. This assumption is presumably slight conservative for an intermeshing rotor, if the reduction of the vortex ring state effects for coaxial rotors is considered according to Ref. 20.

The vertical velocity of the upper boundary w_{BU} and lower boundary w_{BL} are calculated by

$$w_{BU} = v_{iH}\left(\frac{V_{zN}+V_{zX}}{2} + \frac{V_{zN}-V_{zX}}{2}\left(1-\left(\frac{\sqrt{u^2+v^2}}{V_{xM}v_{iH}}\right)^2\right)^{0,2}\right), \quad (15)$$

$$w_{BL} = v_{iH}\left(\frac{V_{zN}+V_{zX}}{2} - \frac{V_{zN}-V_{zX}}{2}\left(1-\left(\frac{\sqrt{u^2+v^2}}{V_{xM}v_{iH}}\right)^2\right)^{1,5}\right). \quad (16)$$

Both functions are scaled with the induced velocity in hover v_{iH}. The following parameters and values are suggested by Johnson in Ref. 16: V_{zN} = -0,45; V_{zX} = -1,5; V_{xM} = 0,95. The formulation is slightly modified with the introduction of the speed components in the body-fixed frame, they are indicated by *u* and *v*. The indicator is calculated as a function of the *w* component of the helicopter speed vector, with a polynomial function of third order. The used four sampling points are shown in the Table 2.

Table 2: Polynomial sampling points for the vortex ring state indicator

w	$w_{BU}+v_{iH}$	w_{BU}	w_{BL}	$w_{BL}-v_{iH}$
Indicator value	0.1	1	1	0.1

As shown in Figure 5 the vortex ring state indicator shows a continuous behavior at the indicator values greater than 0.

In case of a below zero result of the polynomial function the indicator is set to zero.

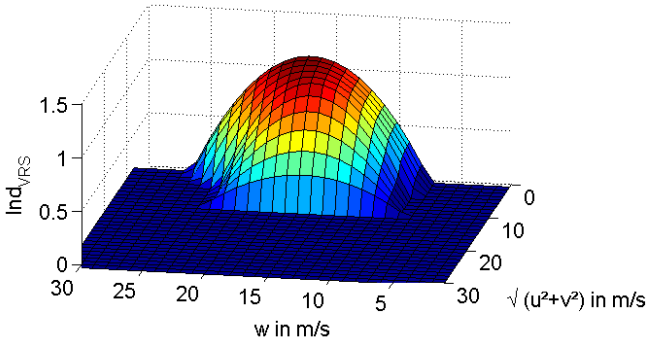

Figure 5: Vortex ring state indicator

In Figure 5 the result of the polynomial function is presented. The velocities of the helicopter in the body fixed frame are denoted as u, v, w.

VERIFICATION OF THE METHOD

The main focus of the simulation study presented in the following is to gain a better understanding of the flight envelope limiting effects. It also serves to evaluate the potential benefit of a more extensive flight envelope expansion campaign for the superARTIS. For this study, the stationary and dynamic trim calcuations of HOST were used. Each calculated point is defined by horizontal and vertical speed as well as gross weight and load factor as defined in Table 3. The commands and loads are calculated by HOST. For all calculated points the air density (ISA standard at msl) and center of gravity is constant. The trim points are chosen to cover an enlarged flight envelope. A uniform sampling over weight, speed and load factor was used to create the set of trim points to be simulated by HOST.

Table 3: Sampling of trim points

Gross weight in kg	{75, 85}
Horizontal speed in km/h	{0, 2, 4, …, 158, 160}
Vertical speed in m/s	{-3, -2.5, -2, …, 9.5, 10}
Load factor in g	{0, 0.1, 0.2, …, 1.9, 2}

To calculate the trim condition for different load factors three maneuvers are used: For load factors greater than one, the helicopter performs stationary turn and for load factors smaller than one a push-over maneuver was simulated. Load factors of one correspond to a stationary level flight.

As a first verification of the approach, two different envelopes are plotted. The vertical over horizontal speed envelope (VC-envelope) is presented, also referred to as climb envelope, see Figure 6 and Figure 7. Furthermore, the load factor over horizontal speed envelope (VN-envelope) is presented in Figure 8. The VN-envelope is also called maneuver envelope due to its main application to limit the loads during high and low load factor maneuvers. These two basic envelopes represent the predominant flight regimes of commercial drones. Climb, descent with different speeds as well as steady turns can be found in these plots. Different altitudes are neglected in this study.

Where not indicated differently, the envelopes are generated using a maximum indicator value Ind_{Max}=90% to define the threshold if a sample is counted to be inside or outside of the flight envelope. In Figure 6 the simulated points of the VC-envelope are shown. The solid line marks the boundary of the calculated envelope. The samples within the flight envelope are colored purple. There are three cases where one single limit indicators is violated defining the boundaries in this example, namely: the power indicator in blue, the control deflection indicator for pitch colored in green, and the vortex ring state indicator in red. The samples were chosen so that the minimal climb rate is 2 m/s thus defining the lower end of the figures.

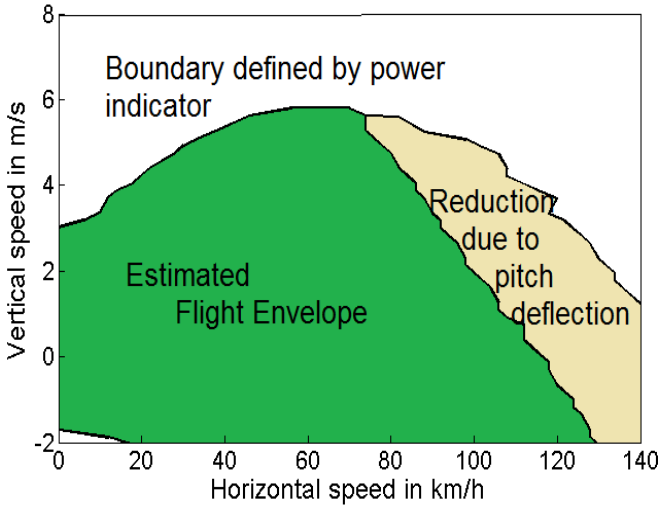

Figure 6: VC-envelope with indicated limits and sampled trim points.

In Figure 7 the VC-envelope is presented for different FEMI thresholds. Generally, the estimated VC-envelope is plausible as the rate of climb increases with an increase of horizontal flight speed up to a plateau at about 60 km/h where the minimum power in forward flight of the superARTIS can be found. After 70 km/h the maximum available climb rate declines. The linear decrease of climb rate after 70 km/h is a result of an actuator control deficit as discussed later. If the actuator deflection limit is mechanically resolved, the FE would be enlarged by the green samples in Figure 6. However, in both cases a reduction of climb rate towards high speed (> 70 km/h) is plausible, but generally caused by engine power limitations. In the example of the superARTIS the actuator deflection limit the maximum level test campaign, see Ref. 6. At speeds below 25 km/h and faster descent rates, the vortex ring state causes a limitation of the flight envelope. The

unsmooth boundary of the FE is a direct result from the sample distances chosen and can be reduced by lowering the step size but increasing the simulation effort.

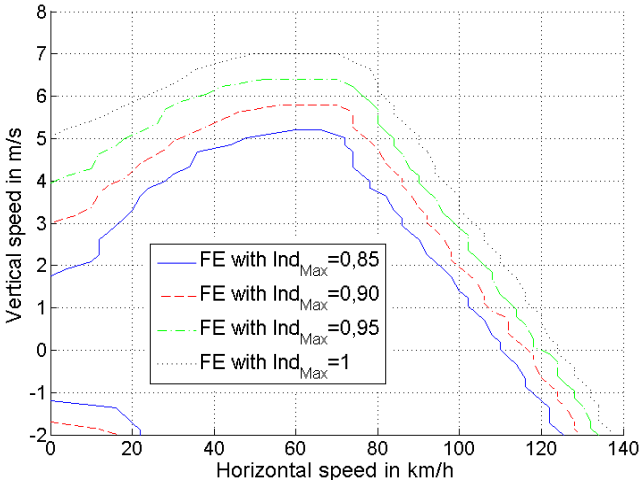

Figure 7: VC-envelope with different indicator limits

In Figure 8, the VN-envelope also represents a plausible flight envelope. For increasing speeds and load factors higher than one the envelope shows a predominantly linear increase motivated by the increasing capability to build up higher load factors due to higher turn speeds. From 80 km/h and faster the sustainable load factors are decreasing until load factors lower than one are reached. Please note, as mentioned before, the different maneuvers used to generate the load-factors. The smaller load factor boundary from 90 to 110 km/h is a range where the HOST was not able to find a valid trim solution with the given trim equilibrium. This can possibly be solved by changing the trim law until a solution can be found as mentioned in Ref. 11.

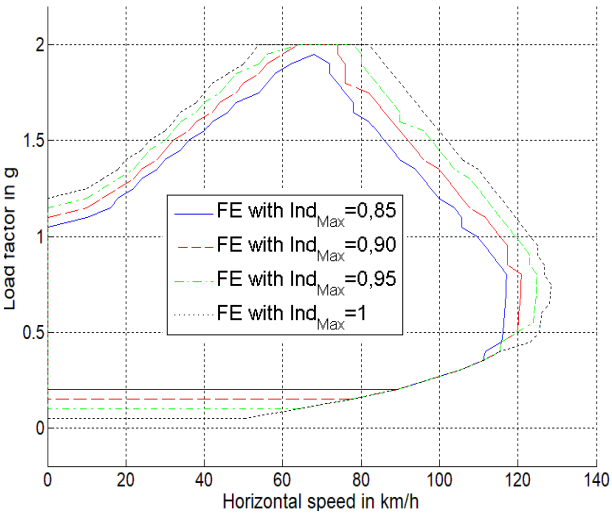

Figure 8: VN-envelope with different indicator limits.

In the following analysis two aspects of the used method will be show. Frist, the ability is demonstrated to determine the limiting effect. Second, the possible improvement in defining the FE in with FEMS in comparison to the static boundaries used on the superARTIS at the moment is presented. For both analyses a maximum indicator value of 90% is used to account for model uncertainties. This empirical indicator value is used for all limit margin indicators and is a result of a comparison of the used HOST model against flight test data of stationary flight conditions.

In Figure 9 and Figure 10 the limiting effects are shown at the FE boundary. The FEs are calculated for a normal operation gross weight of 75 kg. Four of the original six limiting factors are visible. Please note that the hub load and rotor clearance indicators do not limit climb and maneuver envelope and are therefore not shown. Firstly, the power indicator limits the flight performance mainly during climb and low speeds with high turn rates. Secondly, the actuator control authority for the pitch command does limit the higher speeds and corresponding climb rates. Thirdly, the load factor indicator limits maneuver envelope at low load factors up to a speed of about 80 km/h. Fourthly, the vortex ring state indicator limits the climb envelope during low speeds and high descent rates. The remaining boundary component shown is not a physical limitation but, it was not possible to find a valid trim solution at to enlarge the envelope in that section. This is found to be motivated by their dynamic peak response characteristic limiting the occurrence to flight condition with dynamic control inputs. Such peak response limitations rarely limit the flight envelope during steady state operation as mentioned in Ref 21.

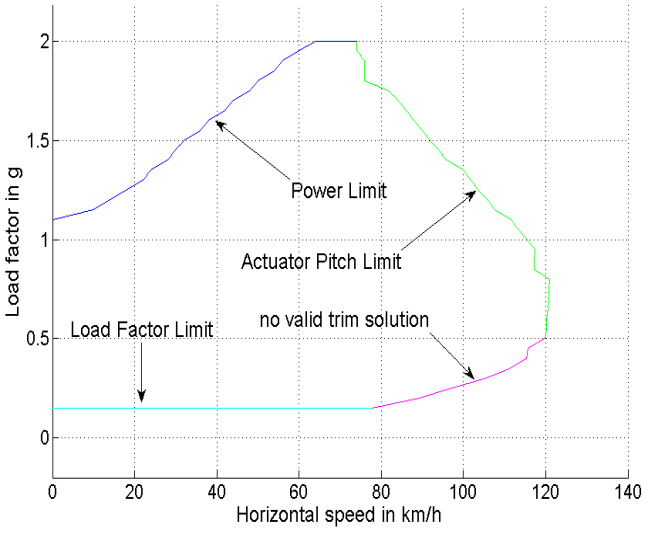

Figure 9: VN-envelope with indicated limits. (Ind_{Max}=90%)

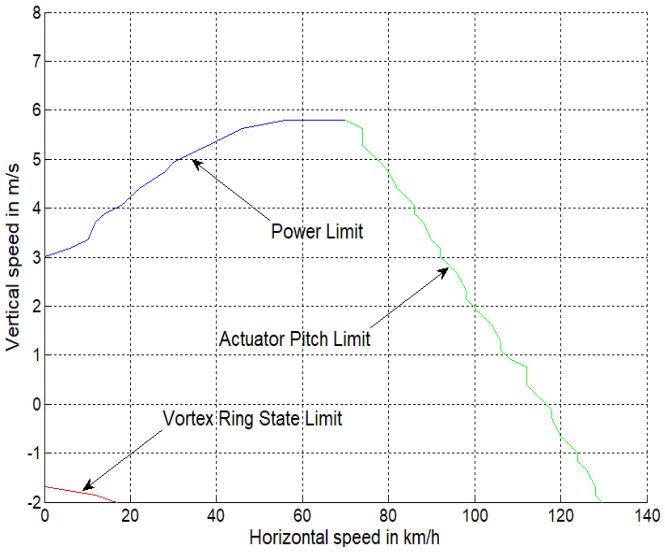

Figure 10: VC-envelope with indicated limits. Ind_{Max}=90%)

In Figure 11 and Figure 12 both maneuver and climb envelopes are shown for 75 and 85 kg gross weight. In the following part of this paper the simulation results are compared to the current flight envelope limitations of the current autopilot(AP).

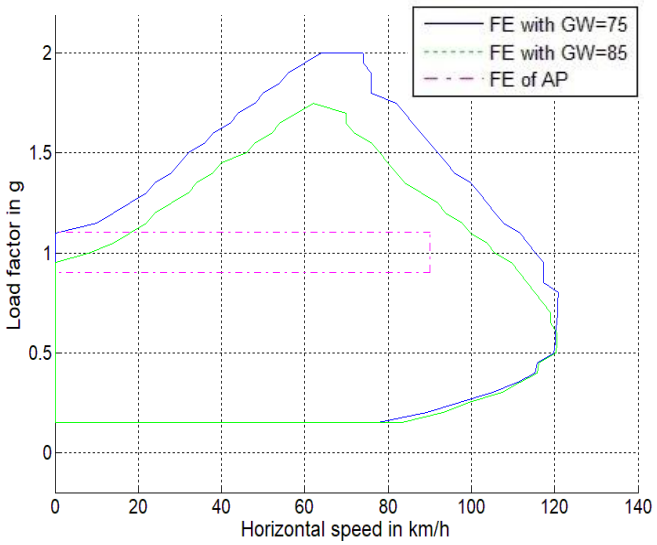

Figure 11: VN-envelopes for 75 and 85 kg gross weight with autopilot boundaries. (Ind_{Max}=90%)

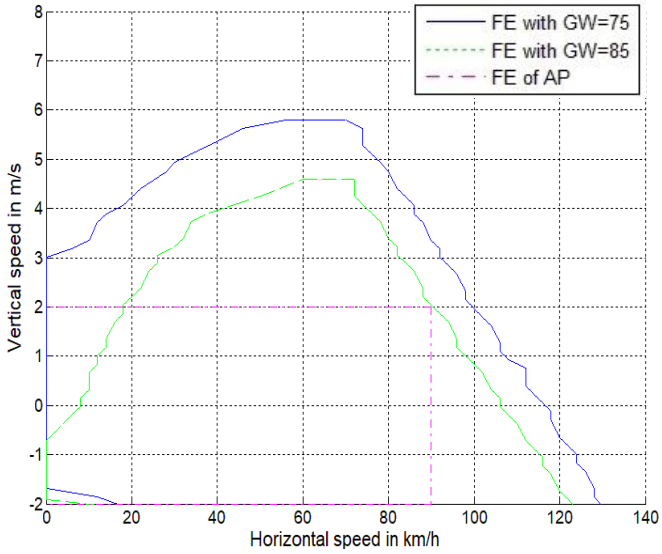

Figure 12: VC-envelopes for 75 and 85 kg gross weight with autopilot boundaries. (Ind_{Max}=90%)

The autopilot limits for the hover condition are very similar to the FE boundaries calculated for 75 kg gross weight. For higher speeds, the autopilot boundaries are generally very conservative in comparison to our 75 kg envelops. The 85 kg VC-FE show that superARTIS cannot hover out of ground effect due to a lack of power. In comparison the autopilot would not protect this critical flight situation.

DISCUSSION AND CONCLUSION

In this paper a method for flight envelope detection is presented. This method is based on a flight mechanic model and a physically motivated calculation of flight envelope limiting effects. The proposed method uses a set of flight envelope indicators, each representing one FE limiting effect. The number of such limit indicators is flexible and can be adapted according to changes of the aircraft or the fidelity of the limit indication. This renders the method advantageous if aircraft configurations change regularly.

The comparison in this paper shows the potential in defining the flight envelope based on physically motivated models instead of using static limits of e.g. speed or bank angle without adapt it to the flight conditions. It shows the potential to utilize improved flight performance during faster forward flight.

It relies on flight mechanic models often used during the design and development phase of unmanned aircraft, this is considered to be less time and money consuming in comparison to pure flight-test based modeling including system identification. However, to use the proposed method, a model validation has to be performed in order to evaluate the model uncertainties. Due to the focus on steady state and the close-to-boundary flight conditions, this validation

process is assumed to be less extensive in comparison to a flight dynamic system identification. Furthermore, the used limit indicator method seems to be useful in flight envelope expansion to find limiting effects and to estimate the potential increase in flight performance.

This method could also answer the question what limiting effect causes a specific part of the boundary. This feature is important for flight envelope expansion. With such information the correct engineering decisions can be made to safely approach each specific part of the flight envelope to unlock the achievable flight performance. The information on the type of the specific limit that is approached reflects on the maneuver used for the flight tests during the expansion process.

The study shows significant potential to improve the unlocked flight performance to DLR's unmanned helicopter superARTIS. As the so far implemented statically defined envelope limits are regularly applied for different types of unmanned aircraft, we expect our method to improve on many UAV applications in the future. More investigation will be needed to assess the reliability of the method. We assume the method should be improved regarding limits that provoke the peak load in the transient state. Another issue to be addressed is an approach for implementation of the method. There are two promising fields. First, the flight envelope protection: using this method and a path optimization method. Second, monitoring and warning of boundaries for the flight envelope expansion process. Therefore, further publications are planned with flight test validation data.

In the future we plan to introduce a hybrid model, consisting of a physically motivated model and an empiric model, to be used as a replacement to HOST to exploit the initial knowledge and improve this baseline with empirical data from each flight performed. Another improvement would be the broadening of the approach to describe the FE boundaries in more dynamic flight conditions, like complex or aggressive maneuvers.

REFERENCES

[1] Geoffrey J. Jeram, *Open Platform for Limit Protection with Carefree Maneuver Application - Dissertation*. Atlanta, GA: Georgia Institude of Technology , 2004.

[2] Ilkay Yavrucuk, "Adaptive Limit Margin Detection and Limit Avoidance," Georgia Institute of Technology, Atlanta, GA, Dissertation 2003.

[3] Gareth D. Padfield, *Helicopter Flight Dynamics*. Oxford, UK: Blackwell Publishing, 2007.

[4] S. Lorenz, "Open-Loop Reference Systems for Nonlinear Control Applied to Unmanned Heliciopters," in *Journal of Guidance, Control, and Dynamics*, Danvers, MA, 2012.

[5] Ilkay Yavrucuk, J.V.R. Prasad, and Surja Unnikrishnan, "Envelope Protection for Autonomous Unmanned Aerial Vehicles," in *AIAA Journal of Guidance, Control, and Dynamics*, Danvers, MA, 2009.

[6] Andreas E. Voigt, Johann C. Dauer, Alex Krenik, and Jörg S. Dittrich, "Detection of Forward Flight Limitations of Unmanned Helicopters," in *American Helicopter Society 72nd Annual Forum*, West Palm Beach, FL, 2016.

[7] Joseph F. Horn, Anthony J. Calise, and J.V.R. Prasad, "Flight Envelope Cueing on a Tilt-Rotor Aircraft Using Neural Network Limit Prediction," in *American Helicopter Society 54th Annual Forum*, Washington, DC, 1999.

[8] Joseph F. Horn, Anthony J. Calise, and J.V.R. Prasad, "Flight Envelope Limiting Systems using Neural Networks," in *AIAA 23rd Atmospheric Flight Mechanic Conference*, Boston, MA, 1998.

[9] Bernard Certain, "The EC 120 Program: Choices, Realization, Results," in *European Rotorcraft Forum and 13th European Helicopter Association Symposium*, Brighton, UK, 1996.

[10] Joseph F. Horn, Anthony J. Calise, and J.V.R. Prasad, "Flight Envelope Limit Detection and Avoidance for Rotorcraft," in *Journal of the American Helicopter Society* , 2002.

[11] Bernard Benoit, Konstantin Kampa, Wolfgang Von Grünhagen, Pierre-Marie Basset, and Bernard Gimonet, "HOST, a General Helicopter Simulation Tool for Germany and France," in *American Helicopter Society 56th Annual Forum*, Virginia Beach, VA, 2000.

[12] David W. King, Charles Dabundo, Ronald L. Kisor, and Ashok Agnihotri, "V-22 Load Limiting Control Law Development," in *American Helicopter Society 49th Annual Forum*, St. Louis, MO, 1993.

[13] H. Walgemoed, "Flight Envelope ," in *Flight Test Techniques Series Vol. 14*. Schiphol-Oost, NL: Research and Technology Organisation of NATO, 2005, p. Chapter 12.

[14] Michael W. Mosher, "Rotorcraft Flight Envelope Unique Considerations," in *Flight Test Techniques Series Vol. 14*. Patuxent River, MD: Research and Technology Organisation of NATO, 2005, vol. Vol. 14, p. Chapter 12a.

[15] Andreas E. Voigt, Johann C. Dauer, and Florian Knaak, "Measurement of Blade Deflection of an Unmanned Intermeshing Rotor Helicopter," in *43rd European Rotorcraft Forum*, Milano, IT, 2017.

[16] W Johnson, "Model for Vortex Ring State Influence on Rotorcraft Flight Dynamic," NASA, Moflett Field, CA, Technical Report 2005.

[17] A Böge, *Handbuch Maschinenbau: Grundlagen und Anwendungen der Maschinenbau-Technik*. Heidelberg, DE: Springer Vieweg Verlag, 2017.

[18] J. Villwock and A. Hanau, *Dubbel - Taschenbuch für Maschinenbau*, 25th ed. Berlin, DE: Springer Vieweg,

2018.

[19] C. Bach and R. Baumann, *Elastizität und Festigkeit*. Berlin, DE: Springer, 1924.

[20] Michael P. Kinzel et al., "An Investigation of the Behavior of a Coaxial Rotor in Decent and Ground Effect," in *AIAA Scitech 2019 Forum*, San Diego, CA, 2019.

[21] Joseph F. Horn, Anthony J. Calise, and J.V.R. Prasad, "Flight Envelope Limit Detection and Avoidance," in *25th European Rotorcraft Forum*, Rome, IT, 1999.